Atmos. Chem. Phys. Discuss., 12, 4655–4678, 2012
www.atmos-chem-phys-discuss.net/12/4655/2012/
doi:10.5194/acpd-12-4655-2012

Atmospheric Chemistry and Physics Discussions

Hydration or dehydration: competing effects of upper tropospheric cloud radiation on the TTL water vapor

L. Wu[1,*], H. Su[1], J. H. Jiang[1], and W. G. Read[1]

[1]Jet Propulsion Laboratory, California Institute of Technology, Pasadena, California, USA
[*]now at: Joint Institute for Regional Earth System Science and Engineering, University of California, Los Angeles, California, USA

Received: 14 December 2011 – Accepted: 22 January 2012 – Published: 8 February 2012

Correspondence to: L. Wu (longtao.wu@jpl.nasa.gov)

Published by Copernicus Publications on behalf of the European Geosciences Union.

Abstract

A tropical channel version of the Weather Research and Forecasting (WRF) model is used to investigate the radiative impacts of upper tropospheric clouds on water vapor in the tropical tropopause layer (TTL). The WRF simulations of cloud radiative effects and water vapor in the upper troposphere and lower stratosphere show reasonable agreement with observations, including approximate reproduction of the water vapor "tape recorder" signal. By turning on and off the upper tropospheric cloud radiative effect (UTCRE) above 200 hPa, we find that the UTCRE induces a warming of 0.76 K and a moistening of 9 % in the upper troposphere at 215 hPa. However, the UTCRE cools and dehydrates the TTL, with a cooling of 0.82 K and a dehydration of 16 % at 100 hPa. The enhanced vertical ascent due to the UTCRE contributes substantially to mass transport and the dehydration in the TTL. The hydration due to the enhanced vertical transport is counteracted by the dehydration from adiabatic cooling associated with the enhanced vertical motion. The UTCRE also substantially changes the horizontal winds in the TTL, resulting in shifts of the strongest dehydration away from the lowest temperature anomalies in the TTL. The UTCRE increases in-situ cloud formation in the TTL. A seasonal variation is shown in the simulated UTCRE, with stronger impact in the moist phase from June to November than in the dry phase from December to May.

1 Introduction

Water vapor in the stratosphere plays an important role in the stratospheric radiative budget and chemistry (e.g. Fueglistaler et al., 2009, and references therein). It is widely accepted that the entry of water vapor into the stratosphere is primarily regulated by the interaction of mass transport and dehydration in the tropics. However, considerable debates exist concerning further details of this entry from the tropical tropopause layer (TTL), the transition layer from the troposphere to the stratosphere.

ACPD
12, 4655–4678, 2012

It is suggested that air is transported to the stratosphere by large-scale slow vertical motions associated with clear-sky radiative heating (e.g. Brewer, 1949). Nonetheless, the mass flux associated with the clear sky radiative heating is too slow to support observational rate of troposphere-to-stratosphere transport (TST; e.g. Sherwood and Dessler, 2003). An alternative hypothesis is that the tropical TST is primarily contributed by deep convective overshooting (e.g., Sherwood and Dessler, 2000). Recently, the radiative effect of cirrus clouds is proposed to be a likely mechanism to accelerate the mass transport from the troposphere to the stratosphere (Corti et al., 2005, 2006; Huang and Su, 2008; Tzella and Legras, 2011).

Another debate exists because the entry of stratospheric water vapor is drier than the expected water vapor saturation mixing ratio with respect to zonal-mean temperature in the TTL (Newell and Gould-Stewart, 1981). Holton and Gettelman (2001) suggested that the rapid horizontal advection dehydrates slowly ascending air by repeatly exposing them to the lowest temperature in the TTL. Sherwood and Dessler (2000) postulated that dehydration might be primarily due to deep convective overshooting. However, experiments showed that overshooting convection hydrates rather than dehydrates the tropical lower stratosphere (e.g. Corti et al., 2008). Based on synoptic-scale temperature and wind fields from reanalysis data, trajectory calculations can explain much of the stratospheric water vapor well (Fueglistaler et al., 2005; Schoeberl and Dessler, 2011). Due to the strong temperature dependence of water vapor pressure, dehydration and transport are intrinsically coupled.

Previous studies have demonstrated that upper tropospheric cloud has significant radiative impacts on TTL temperature or mass transport. A single-layer thin cirrus in the TTL warms local atmosphere by absorbing longwave radiation from surface but emitting at a lower temperature, and thus enhances vertical ascent. For multi-layer cirrus clouds, the cloud radiative effect (CRE) is dependent on the contrast of radiative fluxes between the cirrus in the TTL and underlying clouds (e.g. Hartmann et al., 2001). TTL cirrus overlapping thick clouds could radiatively cool the TTL and result in a weakening of vertical ascent. The opaque clouds ($\tau \geq 3$) can warm the TTL by absorbing solar

ACPD
12, 4655–4678, 2012

radiation (Yang et al., 2010). Observational data show an overall warming of the TTL by the CRE (e.g. Su et al., 2009; Yang et al., 2010). With a two-dimension (2-D) model, Rosenfield et al. (1998) showed that the radiative heating of subvisible thin cirrus would result in a warming of 1–2 K and a vertical velocity increase of 0.02–0.04 mm s^{-1} in the TTL. The lower stratosphere is hydrated by as much as 1 ppmv due to the warmer tropopause. However, other studies showed that cirrus radiative effects are complicated. On one hand, cirrus radiative heating drives the cloud lofting. The cirrus can persist for days and the TTL is dehydrated by the freeze-drying process associated with the uplift of the cloud layer (Jensen et al., 1996; Jensen and Pfister, 2004). On the other hand, the cirrus radiative effects can dissipate clouds in several hours if the energy is only used to warm the atmosphere (Jensen et al., 1996). Dinh et al. (2010) suggested that radiative heating of subvisible cirrus has a potential to dehydrate the TTL by conversion of water vapor into ice through convergence of dry air, without involving adiabatic cooling associated with external large-scale uplift. Also, cirrus can be maintained by the circulation thermally forced by the cloud radiative heating.

Since most of the previous modeling studies were based on idealized 2-D framework, a realistic representation of 3-D structure of the TTL is needed to better understand and quantify the radiative impacts of clouds on the TTL water vapor. Driven by reanalysis data, a 3-D tropical channel model is used in this study to investigate the radiative impacts of upper tropospheric (above 200 hPa) clouds on the TTL water vapor. The model configuration is described in Sect. 2. In Sect. 3, the performance of the tropical channel model in representing CRE and water vapor in the TTL is presented in comparison with satellite observations. Section 4 presents the upper tropospheric cloud radiative effects (UTCRE) on the TTL in the model. The physical processes related to the TTL hydration/dehydration by the UTCRE are discussed in Sect. 5. The conclusion is given in Sect. 6.

ACPD
12, 4655–4678, 2012

2 Model configuration

As a state-of-the-art atmospheric simulation system, the Weather Research and Forecasting (WRF) model is suitable for a broad range of applications across scales ranging from meters to thousands of kilometers. The Advanced Research WRF (ARW) model (Skamarock et al., 2008) Version 3.3 is used in this study. Different from the common practice that uses WRF with a regional domain, we configure our model simulation in a "tropical channel" version for this study. As the horizontal transport of water vapor is quite important to understand the dehydration in the upper troposphere and lower stratosphere (UTLS), the "tropical channel" configuration allows for a realistic depiction of tropical circulation in the UTLS. The control simulation (referred to as CTRL) is configured as a "tropical channel" with 50 km horizontal resolution, covering 15° S to 45° N and 180° W to 180° E. The meridional asymmetry is due to a systematic high bias in the Southern Hemispheric (south to 15° S) water vapor simulation in the TTL, which appears to be related to poor representation of the stratospheric circulation in this version of WRF. Periodic boundary condition is used in the east-west direction. The initialization fields and boundary conditions (north-south and lower boundaries) are obtained from the T255 (~79 km) horizontal resolution of ERA-Interim reanalysis data (http://dss.ucar.edu/datasets/ds627.0/), with an update at every 5 days. To minimize the impact of lateral boundary conditions, the simulated results within 10° S–40° N are analyzed with a focus on the inner tropics (10° S–10° N). The model simulation is conducted from 1 September 2004 to 30 November 2008. Analyses are focused on the last four years (1 December 2004 to 30 November 2008) to avoid the impact of initial conditions. With a terrain-following hydrostatic-pressure coordinate, the model top is set at 10 hPa. The model has 49 eta levels in the vertical, including 7–8 levels in the TTL with the vertical resolution of ~0.6 km. Based on the observed large-scale dynamical structures, Fueglistaler et al. (2009) defined the TTL as a layer between 150 hPa (~14 km) and 70 hPa (~18.5 km). In this study, we follow their definition of the TTL, focusing on the 5 pressure levels (147 hPa, 121 hPa, 100 hPa, 83 hPa and 68 hPa) in

ACPD
12, 4655–4678, 2012

the TTL, which are the standard pressure levels for the Aura Microwave Limb Sounder (MLS) data products. Model simulations are interpolated to the MLS standard pressure levels.

The principal physical schemes used in the simulation include the Lin et al. microphysics scheme (Chen and Sun, 2002), the Grell 3-D ensemble cumulus scheme (Grell and Devenyi, 2002), the Rapid Radiative Transfer Model for Global climate models (RRTMG) longwave scheme (Mlawer et al., 1997; Iacono et al., 2000) and the Goddard (Chou and Suarez, 1994) shortwave scheme. In order to investigate the UTCRE, a sensitivity run (referred as to UTNR) is conducted by turning off CRE (both longwave and shortwave) above 200 hPa, with no modifications of cloud contents and other parameters. Thus, the differences between the CTRL and UTNR simulations represent the UTCRE.

3 Model performance

The MLS Level 2 water vapor product V3.3 (Livesey et al., 2011) is used in this study to evaluate the WRF simulated water vapor in the TTL. Launched in July of 2004, the MLS instrument on board the Aura satellite provides global measurement of upper tropospheric and stratospheric water vapor (Waters et al., 2006). The MLS water vapor data in the TTL have a vertical resolution of ~3 km and horizontal resolutions of ~7 km across-track and ~200 km along-track. The measurement uncertainties of water vapor in the TTL are about 4 % to 15 % (Read et al., 2007).

As the water vapor "tape recorder" (the imprint of tropical temperature on water vapor entering the stratosphere; Mote et al., 1996) clearly marks the seasonal cycle in tropical tropopause temperature coupled with vertical ascent, we first examine the simulated water vapor "tape recorder" in the WRF model. As shown in Fig. 1a, the MLS observed water vapor "tape recorder" shows dry anomalies in the first half of a year (from December to May, hereafter referred to as dry phase), and moist anomalies in the second half of a year (from June to November, hereafter referred to as moist phase). Water

ACPD
12, 4655–4678, 2012

vapor is transported from 121 hPa through the stratosphere while the water vapor signals imprinted at the bottom of the stratosphere are maintained for several months. The WRF CTRL simulation (Fig. 1b) captures seasonal variations of water vapor in the TTL, albeit with a smaller magnitude of the anomalies compared to the MLS data. However, the simulated water vapor "tape recorder" travels upward faster than the MLS observations, especially in the stratosphere. The simulated mean all-sky vertical velocity in the inner tropics is 0.67 mm s^{-1} at 100 hPa, somewhat larger than the observed mean vertical velocity about 0.4 mm s^{-1} (Mote et al., 1998).

The MLS water vapor spatial distribution at 100 hPa (Fig. 2a) shows a minimum over the tropical Western Pacific in December-January-February (DJF). In June-July-August (JJA), the tropical Western Pacific and Indian Ocean are relatively dry while two moist regions are shown at mid-latitude over Asia and Central America (Fig. 2b). The WRF CTRL simulation in DJF (Fig. 2c) captures the location of 100 hPa water vapor minimum in the Western Pacific. However, the model simulation is drier than the MLS data over the relatively dry regions while it is moister over the relatively moist regions. The relative distributions of dry and moist regions in JJA are also captured in the model simulation (Fig. 2d). However, the dry regions over the tropical Western Pacific and Indian Ocean shift westward while the moist regions at mid-latitude shift eastward, comparing to the MLS observations. Similar to in DJF, the simulated water vapor over relatively dry regions is drier than MLS, but moister over relatively moist regions in JJA. Averaged over the inner tropics, the MLS (WRF CTRL) water vapor at 100 hPa is 3.29 (3.26) ppmv in DJF and 4.68 (3.88) ppmv in JJA.

The Clouds and Earth's Radiant Energy System (CERES) Synoptic (SYN) product provides observed TOA (top of atmosphere) fluxes at 1° spatial and 3 hourly temporal resolution. The difference of TOA fluxes between all-sky condition and clear-sky condition is referred as the cloud radiative forcing. As the clear-sky shortwave flux data contain a lot of missing values, we use only TOA longwave fluxes from the CERES Aqua SYN1deg-lite_Ed2.6 monthly product (http://ceres.larc.nasa.gov) and the derived longwave cloud forcing (LWCF).

ACPD
12, 4655–4678, 2012

Figure 3 compares the LWCF from the CERES data with the WRF CTRL simulations in DJF and JJA. The WRF simulations reproduce the LWCF distribution and seasonal variations observed by CERES. In DJF, the magnitude of the simulated LWCF (Fig. 3c) is generally smaller than the magnitude of the CERES observations (Fig. 3a). In JJA, the simulated LWCF (Fig. 3d) is smaller over land but larger over ocean, comparing to the CERES data (Fig. 3b). Averaged in the inner tropics, the CERES (WRF CTRL) LWCF is 38.67 (26.69) $W\,m^{-2}$ in DJF and 35.85 (32.42) $W\,m^{-2}$ in JJA.

Overall, the WRF model reasonably reproduces the relative distribution and seasonal variations of CRE and water vapor in the TTL, although the magnitude and location of simulated CRE and water vapor show discrepancies from observations.

4 Radiative effects of upper tropospheric clouds

Figure 4a shows the 4 yr averaged longwave (LW), shortwave (SW) and net (NET) radiative heating rates for in the inner tropics (10° S–10° N). For both the WRF CTRL and UTNR simulations, SW radiation warms in the UTLS while LW radiation warms the TTL but cools the upper troposphere (UT) from 215 hPa to 147 hPa and lower stratosphere above 68 hPa. In total, there is a radiative heating in the TTL and lower stratosphere, but a radiative cooling in the UT. The UTCRE increases radiative heating rate in the UT by both SW and LW radiation (Fig. 4b). In the lower TTL between 147 hPa and 83 hPa, the UTCRE increases radiative heating rate by enhanced LW warming, but decreases radiative heating rate by reduced SW absorption. Above 83 hPa, the UTCRE corresponds to increased LW cooling and little changes in SW fluxes.

Figure 5 shows the height-time cross section of the UTCRE induced differences averaged over the inner tropics. The UTCRE warms and moistens the UT, but cools and dehydrates the TTL at most of the time (Fig. 5a and b). Seasonal variations of the UTCRE induced changes are seen in the TTL water vapor, with intense dehydration in the moist phase and moderate dehydration in the dry phase. The cooling and dehydration in the dry phase also tends to extend higher in the vertical than in the moist

ACPD
12, 4655–4678, 2012

phase. Due to the strong temperature dependence of the water vapor pressure, the tropical-averaged moisture changes (Fig. 5a) follow the temperature changes (Fig. 5b) in the sign, but their magnitudes are not exactly in phase. For example, the maximum cooling occurs in the dry phase, not in the moist phase. Such shift in phase relation of tropical-averaged water vapor and temperature are results of inhomogenous response to the UTCRE as discussed in Sect. 5. On the 4 yr average at 215 hPa, there is a warming of 0.76 K (maximum up to 1.28 K) and a moistening of 9 % (maximum up to 23 % relative to the CTRL run). The warming and moistening gradually weaken with height in the UT. A transition layer from warming and hydration to cooling and dehydration is shown around 147 hPa. Maximum mean cooling and dehydration occur at 100 hPa with an average cooling of 0.82 K (maximum cooling up to 1.97 K in the dry phase) and a dehydration of 16 % (maximum dehydration up to 40 % in the moist phase). Above 100 hPa, the cooling and dehydration gradually weaken with height.

The UTCRE increases the vertical ascent between 215 hPa and 121 hPa, with maximum increase of vertical velocity at 215 hPa and intense (moderate) enhancement in the moist (dry) phase (Fig. 5c). On the 4 yr average, the increase of vertical velocity (3.18 mm s^{-1}) by the UTCRE is about 49 % of mean vertical velocity at 215 hPa in the CTRL simulation (6.50 mm s^{-1}). On the domain averages between 100 hPa and 83 hPa, the UTCRE increases vertical velocities in DJF, but decreases them in JJA (Figs. 5c and 6). The domain-averaged change of vertical velocity tends to extend higher in the dry phase, corresponding to the higher cooling and dehydration in the dry phase in the TTL. The UTCRE results in slight subsidence above 83 hPa. For ice water content (IWC), the UTCRE mainly increases clouds in the UT and lower TTL (Fig. 5d), especially in the moist phase, while it decreases clouds at some of the time around DJF.

ACPD
12, 4655–4678, 2012

5 Discussion

The thermodynamic energy balance in the TTL can be approximately represented by:

$$\frac{\partial T}{\partial t} + wS = Q \quad (1)$$

where T is temperature; w is vertical velocity; S is static stability; Q is diabatic heating rate (Holton et al., 1995). Based on the thermodynamic energy equation, the net diabatic heating is balanced by the adiabatic ascent and the temperature tendency. Considering the 4 yr-averaged tropical changes in our simulations, the increased radiative heating rate by the UTCRE (Fig. 4b) induces warming and ascent in the UT (Fig. 5b and c). The warming increases the threshold for ice formation in the UT while the enhanced upwelling transports more moisture from below. As a result, moisture increases in the UT (Fig. 5a). Clouds also increase (Fig. 5d), probably related to enhanced vertical transport of ice particles and stronger convective updraft. From 147 hPa to 121 hPa, relatively smaller radiative heating than the UT (Fig. 4b) associated with larger static stability causes weaker increase of ascent. The enhanced adiabatic cooling leads to temperature decrease in this layer of long radiative relaxation time scale. Moisture decreases in response to decreased temperature. Cloud increases (Fig. 5d) are contributed by both vertical transport and freeze-drying processes. Above 83 hPa, the decreased radiative heating rate by the UTCRE (Fig. 4b) is balanced by slight decrease of vertical motion, which leads to cooling and continued dehydration (Fig. 5).

Detailed examination of variations indicates that there are large temporal and spatial departures from the simple explanation between 100 hPa and 83 hPa. Considering the seasonal variations, as shown by the time series of the UTCRE induced monthly averaged differences at 100 hPa (Fig. 6), the change of IWC agrees well with the temperature change. The UTCRE induced cooling increases cloud formation in the TTL. However, the magnitude of water vapor change is not exactly in phase with the magnitude of temperature change. The large discrepancies between the magnitude of temperature and water vapor changes are largely corresponding to the UTCRE induced

ACPD
12, 4655–4678, 2012

changes of vertical water vapor transport ($-\frac{\partial(wq)}{\partial z}$; purple line in Fig. 6). The dehydration from the freeze-drying process is counteracted by the UTCRE enhanced vertical transport at 100 hPa, which results in the phase shift between temperature and water vapor changes. However, the domain-averaged difference in vertical velocity at 100 hPa between the CTRL and UTNR runs changes sign from DJF to JJA, which does not explain the persistently enhanced vertical transport of water vapor throughout the 4 yr. This points to the need to examine spatial variations as shown in Fig. 7.

The seasonal maps of the UTCRE induced differences at 100 hPa are displayed in Fig. 7. In both DJF and JJA, the UTCRE mainly enhances ascent (Fig. 7a and b) in cloudy regions (see Fig. 3c and d). The UTCRE induces subsidence to the west of cloudy regions (Fig. 7a and b) due to wave response (Gill, 1980; Rodwell and Hoskins, 1996). In JJA, more intense downward motion is shown in the inner tropics than in DJF (Fig. 7b), which results in the domain-averaged reduction of vertical ascent at 100 hPa in JJA (Fig. 6). Adiabatic cooling (warming) is associated with the UTCRE induced ascent (descent), with maximum cooling (warming) shifted to the west of the maximum ascent (descent) due to horizontal advection. Except over the Indian Ocean, dehydration by the UTCRE corresponds to cooling in most regions, with maximum dehydration shown at the Western Pacific around 20° N (Fig. 7c and d). Over the Indian Ocean, the UTCRE induces strong westerly anomalies (weakening of easterly) in DJF and strong easterly anomalies in JJA. The strong wind anomalies carry dehydrated air downstream away from the origin that dehydration takes place, resulting in offsets of the locations of the driest and coldest anomalies. Thus, less dehydration (hydration around the descent in DJF) is shown over the Indian Ocean in both DJF and JJA although cold anomalies over the Indian Ocean are stronger than over Western Pacific (Fig. 7a and b). Similarly, the increase of clouds is shifted away from the strongest negative temperature anomalies due to horizontal advection by anomalous winds (Fig. 7e and f). Less cloud increase occurs over the Indian Ocean comparing to Western Pacific.

Hence, the argument is still valid at 100 hPa, where the enhanced updrafts in cloudy regions induce adiabatic cooling and dehydration in both DJF and JJA. However, strong

ACPD
12, 4655–4678, 2012

descent anomaly to the west of ascent are induced by the UTCRE at 100 hPa (Fig. 7b), which leads to decrease of vertical velocity in JJA in the domain-averages (Figs. 5c and 6). The dehydration by adiabatic cooling is counteracted by the enhanced vertical transport of water vapor at 100 hPa, which results in that the magnitude of water vapor changes is not following the magnitude of temperature changes (Fig. 6). Due to significant changes of horizontal winds (mainly around Indian Ocean) induced by the UTCRE, the maximum UTCRE induced cooling is not collocated with the maximum dehydration.

6 Conclusions

In this study, we implement the "tropical channel" configuration of the WRF model to investigate the radiative impacts of upper tropospheric clouds (all clouds above 200 hPa) on the TTL water vapor. The 4 yr WRF simulations show reasonable agreements with observations on CRE and water vapor in the TTL, including approximate reproduction of the water vapor "tape recorder" in the TTL.

Sensitivity experiment demonstrates that the UTCRE increases temperature and vertical motion in the UT from 215 hPa to 147 hPa. On the 4 yr average at 215 hPa, the UTCRE contributes to a warming of 0.76 K and enhanced updraft by 49 % in the WRF CTRL run. The significant warming and enhanced vertical transport lead to increase of both water vapor (increase by 9 % at 215 hPa) and clouds in the UT. In the lower TTL from 147 hPa to 83 hPa, increase of upwelling by the UTCRE contributes to enhanced vertical transport of water vapor. However, the enhanced vertical motion is associated with increased adiabatic cooling, which dehydrates the lower TTL by forming more ice clouds. The dehydration by adiabatic cooling offsets the hydration by the enhanced vertical transport and results in a net dehydration in the lower TTL. On the 4 yr average, the simulated UTCRE leads to a maximum cooling of 0.82 K and a maximum dehydration of 16 % at 100 hPa. The cloud radiative cooling induces reduction of the ascent rate, temperature decrease and dehydration above 83 hPa.

ACPD
12, 4655–4678, 2012

On the 4 yr averaged vertical profiles in the inner tropics, the change of water vapor shows strong dependence on the temperature change. However, the magnitude of water vapor changes is not in phase with the magnitude of temperature changes due to the competing effect of enhanced vertical transport of water vapor by the UTCRE. Moreover, the maps at 100 hPa show that the maximum dehydration is not collocated with the maximum cooling. The UTCRE induced temperature change has substantial horizontal and vertical variations over the tropics. At 100 hPa, the UTCRE generally induces ascent in cloudy regions and descent to the west of ascent. The UTCRE induced anomalous horizontal advection over Indian Ocean transports water vapor anomalies away from the lowest temperature anomalies. Due to horizontal advection, the maximum cooling is also located west of the maximum ascent anomaly in the tropics.

This study confirms that the radiative impacts of upper tropospheric clouds contribute substantially to tropical TST (Corti et al., 2005, 2006). Moreover, the UTCRE has significant impact on the dehydration in the TTL. The UTCRE also helps cloud formation in the TTL. Thus, an accurate representation of the UTCRE is needed in order to have a realistic water vapor and energy budget in the UTLS. Recent studies indicate aerosols may interact with UT clouds to affect TTL water vapor through radiative and microphysical processes (Su et al., 2011; Wu et al., 2011), further pointing to the importance of continued study of UTCRE on TTL mass transport.

Our analysis also shows that horizontal transport is quite important to dehydration in the TTL. It is insufficient to investigate dehydration simply based on temperature without consideration of the large-scale circulation. As pointed out by previous studies (Fueglistaler et al., 2005; Tzella and Legras, 2011), a representation of large-scale circulation is necessary to well quantify the dehydration processes in the TTL.

Some caveats in this study should be noted. First, the simulated water vapor "tape recorder" travels upward faster than the MLS observations, especially in the stratosphere. The stratospheric Brewer-Dobson circulation is one of the most important factors contributed to the "tape recorder" signal and transport in the stratosphere

ACPD
12, 4655–4678, 2012

(Fueglistaler et al., 2009, and references therein). The simulated fast transport in the stratosphere might be due to the model top setting at 10 hPa, which cannot fully resolve the Brewer-Dobson circulation. Secondly, in the inner tropics, the CERES data have larger cloud forcing in DJF than in JJA. Although the model simulation captures the distribution of TOA LWCF as in CERES, it produces larger cloud forcing in JJA than in DJF. Due care should be used when interpreting the seasonal variation and magnitude of the UTCRE.

Acknowledgements. The authors thank Leonhard Pfister for valuable discussions. This study was supported by NASA Aura Science Team program, as well as the Aura MLS project. The work is conducted at the Jet Propulsion Laboratory, California Institute of Technology, under contract with NASA. The JPL author's copyright for this publication is held by the California Institute of Technology. Government Sponsorship acknowledged.

References

Brewer, A. W.: Evidence for a world circulation provided by the measurements of helium and water vapour distribution in the stratosphere, Q. J. Roy. Meteor. Soc., 75, 351–363, 1949.

Chen, S.-H. and Sun, W.-Y.: A one-dimensional time dependent cloud model, J. Meteorol. Soc. Japan, 80, 99–118, 2002.

Chou, M.-D. and Suarez, M. J.: An efficient thermal infrared radiation parameterization for use in general circulation models, NASA Tech. Memo., 104606, 3, 85 pp., 1994.

Corti, T., Luo, B. P., Peter, T., Vömel, H., and Fu, Q.: Mean radiative energy balance and vertical mass fluxes in the equatorial upper troposphere and lower stratosphere, Geophys. Res. Lett., 32, L06802, doi:10.1029/2004GL021889, 2005.

Corti, T., Luo, B. P., Fu, Q., Vömel, H., and Peter, T.: The impact of cirrus clouds on tropical troposphere-to-stratosphere transport, Atmos. Chem. Phys., 6, 2539–2547, doi:10.5194/acp-6-2539-2006, 2006.

Corti, T., Luo, B. P., de Reus, M., Brunner, D., Cairo, F., Mahoney, M. J., Martucci, G., Matthey, R., Mitev, V., dos Santos, F. H., Schiller, C., Shur, G., Sitnikov, N. M., Spelten, N., Vössing, H. J., Borrmann, S., and Peter, T.: Unprecedented evidence for deep convection hydrating the tropical stratosphere, Geophys. Res. Lett., 35, L10810, doi:10.1029/2008GL033641, 2008.

ACPD

12, 4655–4678, 2012

Dinh, T. P., Durran, D. R., and Ackerman, T. P.: Maintenance of tropical tropopause layer cirrus, J. Geophys. Res., 115, D02104, doi:10.1029/2009JD012735, 2010.
Fueglistaler, S., Bonazzola, M., Haynes, P. H., and Peter, T.: Stratospheric water vapor predicted from the Lagrangian temperature history of air entering the stratosphere in the tropics, J. Geophys. Res., 110, D08107, doi:10.1029/2004JD005516, 2005.
Fueglistaler, S., Dessler, A. E., Dunkerton, T. J., Folkins, I., Fu, Q., and Mote, P. W.: Tropical tropopause layer, Rev. Geophys., 47, RG1004, doi:10.1029/2008RG000267, 2009.
Gill, A. E.: Some simple solutions for heat-induced tropical circulation, Q. J. Roy. Meteor. Soc., 106, 447–462, 1980.
Grell, G. A. and Dévényi, D.: A generalized approach to parameterizing convection combining ensemble and data assimilation techniques, Geophys. Res. Lett., 29, 1693, doi:10.1029/2002GL015311, 2002.
Hartmann, D. L., Holton, J. R., and Fu, Q.: The heat balance of the tropical tropopause, cirrus, and stratospheric dehydration, Geophys. Res. Lett., 28, 1969–1972, doi:10.1029/2000GL012833, 2001.
Holton, J. R. and Gettelman, A.: Horizontal transport and the dehydration of the stratosphere, Geophys. Res. Lett., 28, 2799–2802, 2001.
Holton, J. R., Haynes, P. H., McIntyre, M. E., Douglass, A. R., Rood, R. B., and Pfister, L.: Stratosphere-troposphere exchange, Rev. Geophys., 33, 403–439, doi:10.1029/95RG02097, 1995.
Huang, X. and Su, H.: Cloud radiative effect on tropical troposphere to stratosphere transport represented in a large-scale model, Geophys. Res. Lett., 35, L21806, doi:10.1029/2008GL035673, 2008.
Iacono, M. J., Mlawer, E. J., Clough, S. A., and Morcrette, J.-J.: Impact of an improved longwave radiation model, RRTM, on the energy budget and thermodynamic properties of the NCAR community climate model, CCM3, J. Geophys. Res., 105, 14873–14890, doi:10.1029/2000JD900091, 2000.
Jensen, E. and Pfister, L.: Transport and freeze-drying in the tropical tropopause layer, J. Geophys. Res., 109, D02207, doi:10.1029/2003JD004022, 2004.
Jensen, E. J., Toon, O. B., Pfister, L., and Selkirk, H. B.: Dehydration of the upper troposphere and lower stratosphere by subvisible cirrus clouds near the tropical tropopause, Geophys. Res. Lett., 23, 825–828, doi:10.1029/96GL00722, 1996.
Livesey, N. J., Read, W. J., Froidevaux, L., Lambert, A., Manney, G. L., Pumphrey, H. C.,

ACPD
12, 4655–4678, 2012

Santee, M. L., Schwartz, M. J., Wang, S., Cofield, R. E., Cuddy, D. T, Fuller, R. A., Jarnot, R. F., Jiang, J. H., Knosp, B. W., Stek, P. C., Wagner, P. A., and Wu, D. L.: EOS Aura Microwave Limb Sounder Version 3.3 Level 2 data quality and description document, JPL document, D-33509, 2011.

Mlawer, E. J., Taubman, S. J., Brown, P. D., Iacono, M. J., and Clough, S. A.: Radiative transfer for inhomogeneous atmosphere: RRTM, a validated correlated-k model for the longwave, J. Geophys. Res., 102, 16663–16682, 1997.

Mote, P., Dunkerton, T., McIntyre, M., Ray, E., Haynes, P., and Russell III, J.: Vertical velocity, vertical diffusion, and dilution by midlatitude air in the tropical lower stratosphere, J. Geophys. Res., 103, 8651–8666, 1998.

Mote, P., Rosenlof, K., McIntyre, M., Carr, E., Gille, J., Holton, J., Kinnersley, J., Pumphrey, H., Russell III, J., and Waters, J.: An atmospheric tape recorder: The imprint of tropical tropopause temperatures on stratospheric water vapor, J. Geophys. Res., 101, 3989–4006, 1996.

Newell, R. E. and Gould-Stewart, S.: A Stratospheric Fountain?, J. Atmos. Sci., 38, 2789–2796, 1981.

Read, W. G., Lambert, A., Bacmeister, J., Cofield, R. E., Christensen, L. E., Cuddy, D. T., Daffer, W. H., Drouin, B. J., Fetzer, E., Froidevaux, L., Fuller, R., Herman, R., Jarnot, R. F., Jiang, J. H., Jiang, Y. B., Kelly, K., Knosp, B. W., Kovalenko, L. J., Livesey, N. J., Liu, H.-C., Manney, G. L., Pickett, H. M., Pumphrey, H. C., Rosenlof, K. H., Sabounchi, X., Santee, M. L., Schwartz, M. J., Snyder, W. V., Stek, P. C., Su, H., Takacs, L. L., Thurstans, R. P., Vömel, H., Wagner, P. A., Waters, J. W., Webster, C. R., Weinstock, E. M., and Wu, D. L.: Aura Microwave Limb Sounder upper tropospheric and lower stratospheric H_2O and relative humidity with respect to ice validation, J. Geophys. Res., 112, D24S35, doi:10.1029/2007JD008752, 2007.

Rodwell, M. J. and Hoskins, B. J.: Monsoons and the dynamics of deserts, Q. J. Roy. Meteor. Soc., 122, 1385–1404, 1996.

Rosenfield, J. E., Considine, D. B., Schoeberl, M. R., and Browell, E. V.: The impact of subvisible cirrus clouds near the tropical tropopause on stratospheric water vapor, Geophys. Res. Lett., 25, 1883–1886, doi:10.1029/98GL01294, 1998.

Schoeberl, M. R. and Dessler, A. E.: Dehydration of the stratosphere, Atmos. Chem. Phys., 11, 8433–8446, doi:10.5194/acp-11-8433-2011, 2011.

Sherwood, S. C. and Dessler, A. E.: On the control of stratospheric humidity, Geophys. Res. Lett., 27, 2513–2516, 2000.

ACPD
12, 4655–4678, 2012

Sherwood, S. C. and Dessler, A. E. L: Convective Mixing near the Tropical Tropopause: Insights from Seasonal Variations, J. Atmos. Sci., 60, 2674–2685, 2003.
Skamarock, W. C., Klemp, J. B., Dudhia, J., Gill, D. O., Barker, D. M., Wang, W., and Powers, J. G.: A Description of the Advanced Research WRF Version 3, NCAR Technical Note TN-468+STR, 113 pp., 2008.
Su, H., Jiang, J. H., Stephens, G. L., Vane, D. G., and Livesey, N. J.: Radiative effects of upper tropospheric clouds observed by Aura MLS and CloudSat, Geophys. Res. Lett., 36, L09815, doi:10.1029/2009GL037173, 2009.
Su, H., Jiang, J. H., Liu, X., Penner, J. E., Read, W. G., Massie, S., Schoeberl, M. R., Colarco, P., Livesey, N. J., and Santee, M. L.: Observed increase of TTL temperature and water vapor in polluted clouds over Asia, J. Climate, 24, 2728–2736, doi:10.1175/2010JCLI3749.1, 2011.
Tzella, A. and Legras, B.: A Lagrangian view of convective sources for transport of air across the Tropical Tropopause Layer: distribution, times and the radiative influence of clouds, Atmos. Chem. Phys., 11, 12517–12534, doi:10.5194/acp-11-12517-2011, 2011.
Waters, J. W., Froidevaux, L., Harwood, R. S., Jarnot, R. F., Pickett, H. M., Read, W. G., Siegel, P. H., Cofield, R. E., Filipiak, M. J., Flower, D. A., Holden, J. R., Lau, G. K., Livesey, N. J., Manney, G. L., Pumphrey, H. C., Santee, M. L., Wu, D. L., Cuddy, D. T., Lay, R. R., Loo, M. S., Perun, V. S., Schwartz, M. J., Stek, P. C., Thurstans, R. P., Boyles, M. A., Chandra, K. M., Chavez, M. C., Chen, G.-S., Chudasama, B. V., Dodge, R., Fuller, R. A., Girard, M. A., Jiang, J. H., Jiang, Y., Knosp, B. W., Labelle, R. C., Lam, J. C., Lee, A. K., Miller, D., Oswald, J. E., Patel, N. C., Pukala, D. M., Quintero, O., Scaff, D. M., Vansnyder, W., Tope, M. C., Wagner, P. A., and Walch, M. J.: The Earth Observing System Microwave Limb Sounder (EOS MLS) on the Aura satellite, IEEE Trans, Geosci. Remote Sens., 44, 1075–1092, doi:10.1109/TGRS.2006.873771, 2006.
Wu, L., Su, H., and Jiang, J. H.: Regional simulations of deep convection and biomass burning over South America – Part 2: Biomass burning aerosol effects on clouds and precipitation, J. Geophys. Res., 116, D17209, doi:10.1029/2011JD016106, 2011.
Yang, Q., Fu, Q., and Hu, Y.: Radiative impacts of clouds in the tropical tropopause layer, J. Geophys. Res., 115, D00H12, doi:10.1029/2009JD012393, 2010.

ACPD
12, 4655–4678, 2012

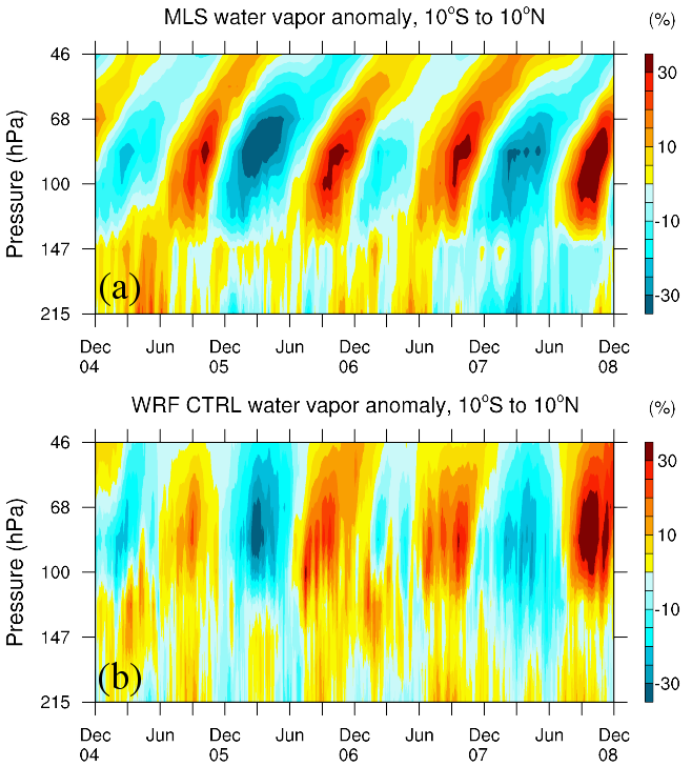

Fig. 1. Height-time cross section of inner tropical (10° S–10° N) mean water vapor anomalies from **(a)** MLS and **(b)** the WRF CTRL run. The anomalies are relative to inner tropical mean averaged from 1 December 2004 to 30 November 2008.

ACPD
12, 4655–4678, 2012

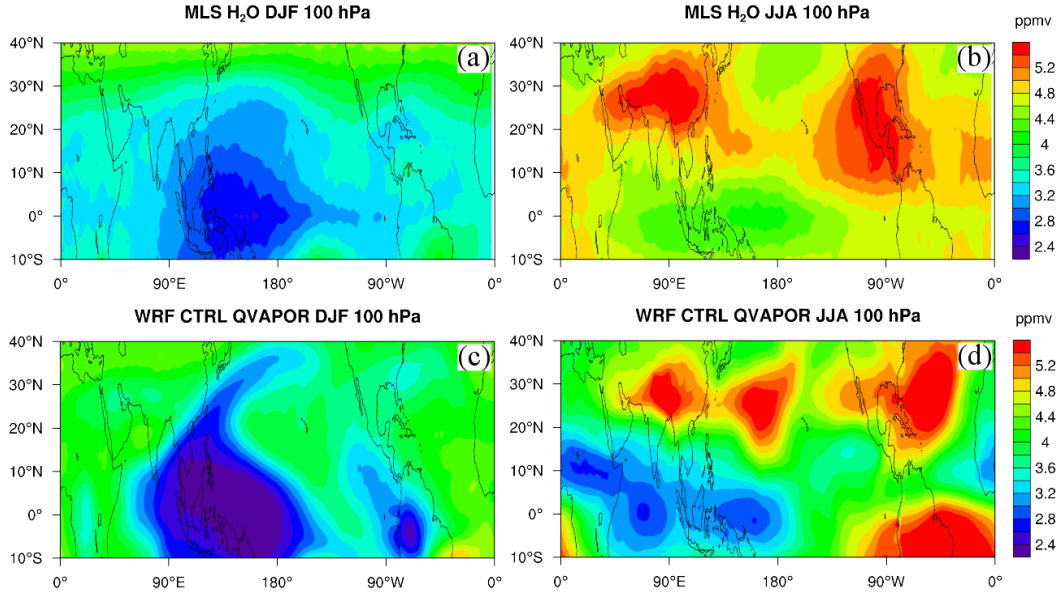

Fig. 2. 4 yr averaged water vapor (ppmv) at 100 hPa. **(a)** MLS in DJF; **(b)** MLS in JJA; **(c)** WRF CTRL in DJF; **(d)** WRF CTRL in JJA.

ACPD
12, 4655–4678, 2012

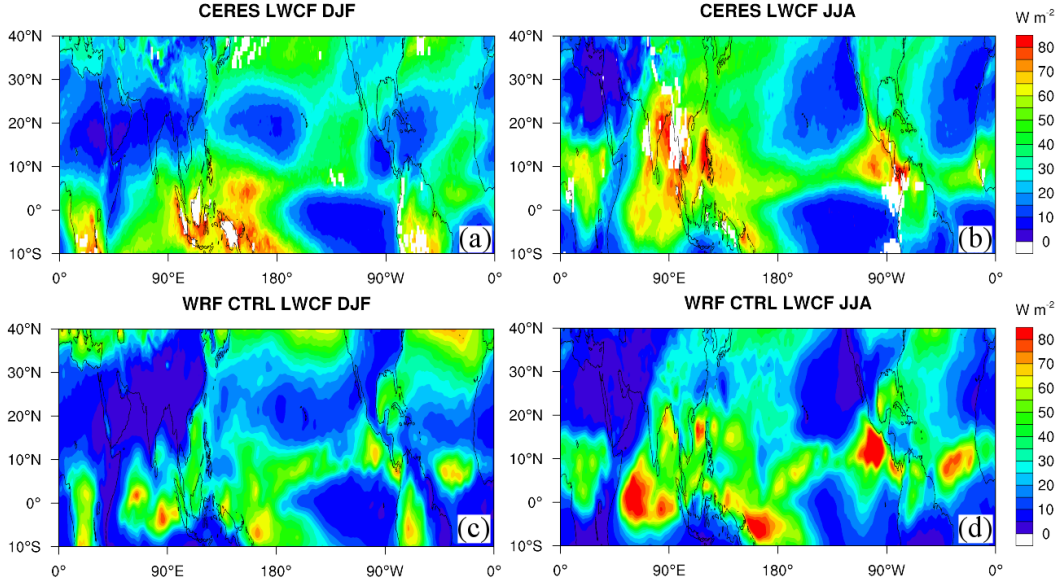

Fig. 3. 4 yr averaged LWCF ($W\,m^{-2}$) at the TOA. **(a)** CERES in DJF; **(b)** CERES in JJA; **(c)** WRF CTRL in DJF; **(d)** WRF CTRL in JJA.

ACPD
12, 4655–4678, 2012

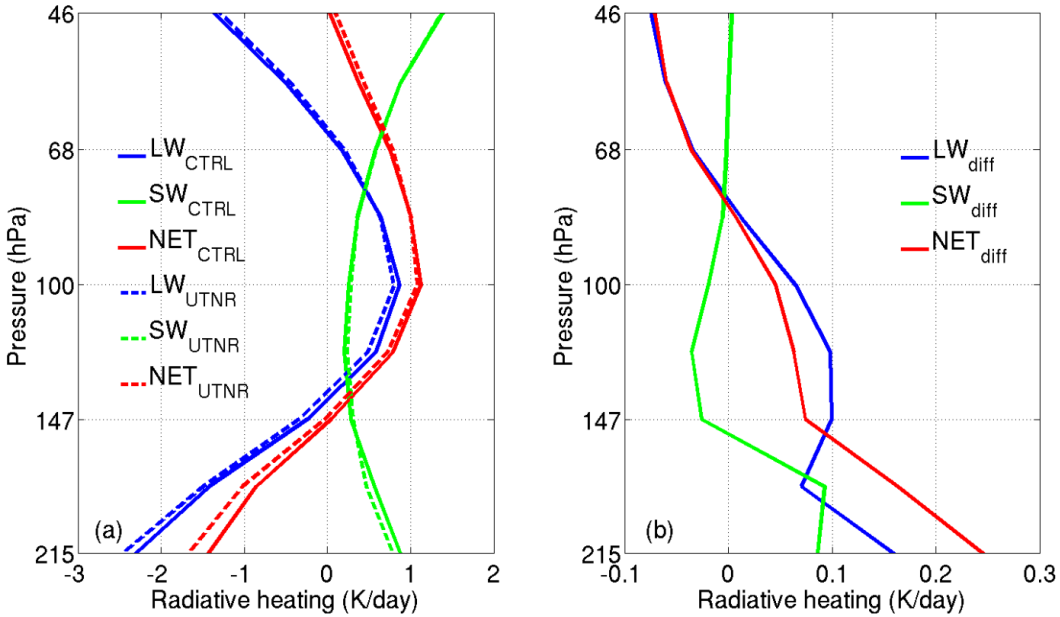

Fig. 4. **(a)** 4 yr averaged cloud radiative heating rates (K day^{-1}) in the inner tropics (10° S–10° N). Solid (dashed) blue is LW cloud radiative heating in the WRF CTRL (UTNR) run. Solid (dashed) green is SW cloud radiative heating in the WRF CTRL (UTNR) run. Solid (dashed) red is the net (NET) of SW and LW cloud radiative heating in the WRF CTRL (UTNR) run. **(b)** 4 yr-averaged differences of cloud radiative heating rates (K day^{-1}) in the inner tropics for LW (blue), SW (green) and NET (red).

ACPD
12, 4655–4678, 2012

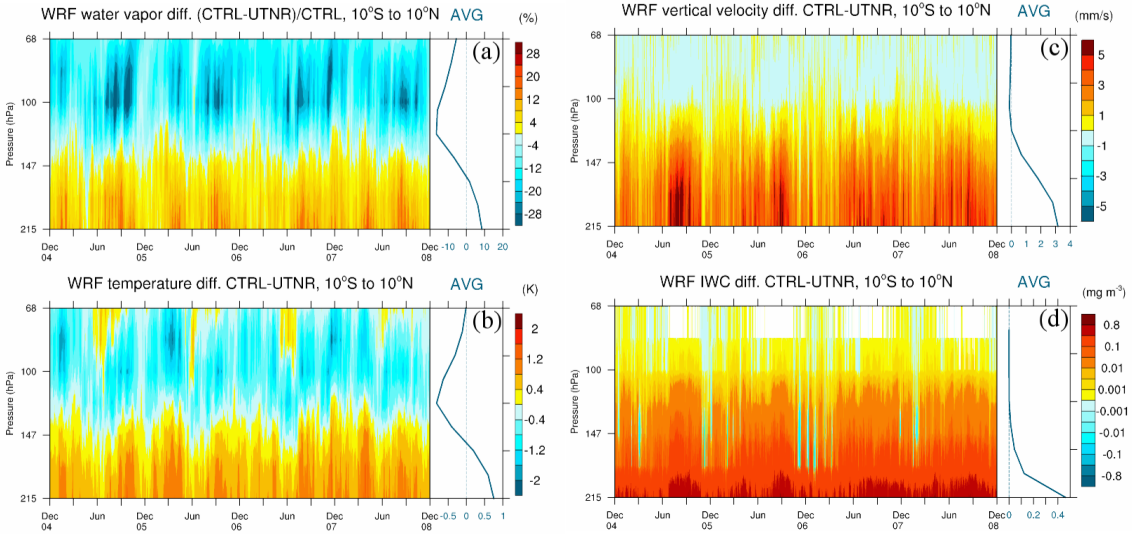

Fig. 5. (left panel) Height-time cross section of inner tropical (10° S–10° N) mean daily differences between the WRF CTRL and UTNR simulations for **(a)** water vapor difference (%) relative to the WRF CTRL run; **(b)** temperature difference (K); **(c)** vertical velocity difference (mm s^{-1}); **(d)** IWC difference (mg m^{-3}). (right panel) Vertical profiles of 4 yr mean differences in left panel.

ACPD
12, 4655–4678, 2012

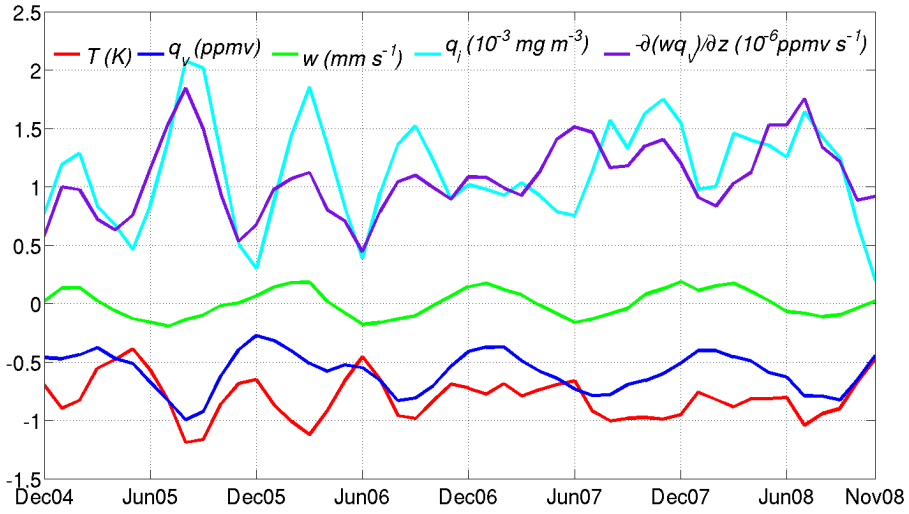

Fig. 6. The time series of monthly averaged differences at 100 hPa. Temperature difference (K) in red; water vapor (ppmv) difference in blue; vertical velocity (mm s^{-1}) difference in green; ice water content (10^{-3} mg m^{-3}) in cyan; vertical water vapor flux ($-\frac{\partial(wq)}{\partial z}$; 10^{-6} ppmv s^{-1}) in purple.

ACPD
12, 4655–4678, 2012

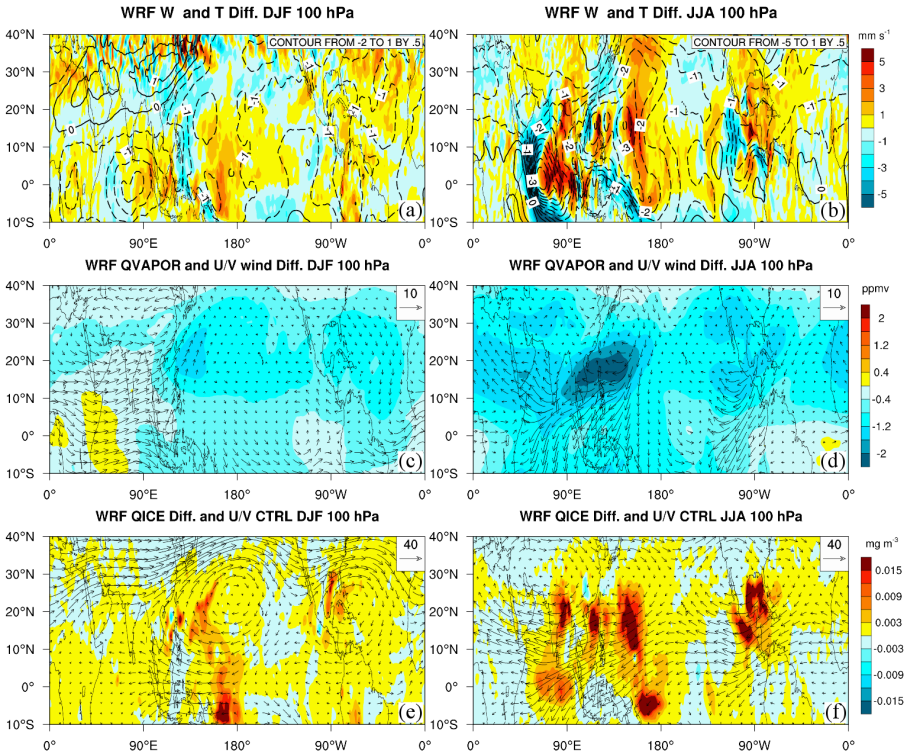

Fig. 7. **(a)** The differences of vertical velocity (shade; mm s^{-1}) and temperature (contour with dashed lines for negative values and solid lines for positive values; K) between the WRF CTRL and UTNR runs at 100 hPa in DJF; **(b)** same as **(a)** but in JJA. **(c)** The differences of water vapor (shade; ppmv) and horizontal wind (vector; m s^{-1}) between the WRF CTRL and UTNR runs at 100 hPa in DJF; **(d)** same as **(c)** but in JJA. **(e)** The horizontal wind (vector; m s^{-1}) in the WRF CTRL run and the difference of cloud ice (shade; mg m^{-3}) between the WRF CTRL and UTNR runs at 100 hPa in DJF; **(f)** same as **(e)** but in JJA.

ACPD
12, 4655–4678, 2012